Ferromagnetic interlayer coupling in $FeSe_{1-x}S_x$ superconductors revealed by inelastic neutron scattering

Mingwei Ma,[1,2,*] Philippe Bourges,[3] Yvan Sidis,[3] Jinzhao Sun,[2,†] Guoqing Wang,[2] Kazuki Iida,[4] Kazuya Kamazawa,[4] Jitae T. Park,[5] Frederic Bourdarot,[6] Zhian Ren,[1] and Yuan Li[2,7,‡]

[1]*Beijing National Laboratory for Condensed Matter Physics, Institute of Physics, Chinese Academy of Sciences, Beijing 100190, China*

[2]*International Center for Quantum Materials, School of Physics, Peking University, Beijing 100871, China*

[3]*Université Paris-Saclay, CNRS, CEA, Laboratoire Léon Brillouin, 91191 Gif-sur-Yvette, France*

[4]*Neutron Science and Technology Centre, Comprehensive Research Organization for Science and Society (CROSS), Tokai, Ibaraki 319-1106, Japan*

[5]*Heinz Maier-Leibnitz Zentrum (MLZ), Technische Universität München, D-85748 Garching, Germany*

[6]*Université Grenoble Alpes, CEA, IRIG, MEM, MDN, 38000 Grenoble, France*

[7]*Collaborative Innovation Center of Quantum Matter, Beijing 100871, China*

(Received 29 June 2024; revised 18 September 2024; accepted 24 October 2024; published 5 November 2024)

$FeSe_{1-x}S_x$ superconductors are commonly considered layered van der Waals materials with negligible interlayer coupling. Here, using inelastic neutron scattering to study spin excitations in single-crystal samples, we reveal that the magnetic coupling between adjacent Fe layers is ferromagnetic in nature, making the system different from most unconventional superconductors including iron pnictides. The weak interlayer coupling is estimated to be $J_c \sim 0.2$ meV, in agreement with the short spin-spin correlation length $\xi_c \sim 0.2c$ along the c axis. The results provide an experimental basis for establishing a microscopic theoretical model to describe the absence of magnetic order in $FeSe_{1-x}S_x$.

DOI: 10.1103/PhysRevB.110.174503

I. INTRODUCTION

A common thread for understanding unconventional superconductivity is magnetic interactions [1–3], about which inelastic neutron scattering (INS) measurements of spin excitations can provide useful information. Since unconventional superconductors are mostly layered materials, a distinct aspect of such information is the nature and strength of interlayer magnetic coupling, as manifested by magnetic excitations' momentum dependence along the $\mathbf{c}^*$ direction. Taking the well-known spin resonance mode [4] as an example, sinusoidal modulation of its intensity along $\mathbf{c}^*$ in Co/Ni-doped $BaFe_2As_2$ [5–7], $NaFe_{0.985}Co_{0.015}As$ [8], and $CeCoIn_5$ [9], as well as its dispersion in $BaFe_2(As_{1-x}P_x)_2$ [10], can be attributed to antiferromagnetic spin correlations or interactions between adjacent quintessential layers of atoms that are responsible for both the superconductivity and the magnetism. Such antiferromagnetic coupling is also found in superconductors with two quintessential layers (i.e., FeAs or Cu_2O layers) within the primitive cell, such as $CaKFe_4As_4$, $YBa_2Cu_3O_{6+\delta}$, and $Bi_2Sr_2CaCu_2O_{8+\delta}$ [11–17]. When the interlayer coupling is negligible, the spin excitations are observed to be nearly independent of momentum transfer along $\mathbf{c}^*$, as found in $FeSe_{0.4}Te_{0.6}$ [18], $Rb_xFe_{2-y}Se_2$ [19], LaOFeAs [20], LiFeAs [21], and $Li_{0.8}Fe_{0.2}ODFeSe$ [22,23].

FeSe is regarded as two-dimensional material as it is composed of a stack of strongly bonded edge-sharing $FeSe_4$-tetrahedra layers, as shown in Figs. 1(d) and 1(e) [24]. The weak van der Waals bonding between the FeSe layers allows the material to easily cleave, and it shows potential for use in heterostructure devices with a tunable superconducting transition temperature T_c above 40 K [25–27]. Additionally, the FeSe layers can be intercalated with different charged or neutral spacer layers, or grown as monolayers on $SrTiO_3$, leading to a significant increase of T_c [28–35]. An unique feature of FeSe is the spontaneous fourfold symmetry breaking observed in the bulk material at the nematic temperature $T_s = 88$ K, driven by electronic or magnetic instabilities. This nematic state, unlike in Fe pnictides, does not exhibit long-range magnetic order under ambient pressure [36]. The absence of magnetic order in FeSe has sparked interest from various perspectives, including orbital physics [37] and quantum magnetism such as the spin-fluctuation-induced spin-quadrupole order [38], the nematic quantum paramagnetic phase [39], the ferro-orbital order in the nematic phase [40], the near degeneracy between magnetic fluctuations and fluctuations in the charge-current density-wave channel [41], as well as the vertex correction [42]. However, there are few discussions of the absence of magnetic order in FeSe from the viewpoint of the interlayer coupling. Here, we study its interlayer coupling revealed by INS and find that the spin resonance mode is highly modulated along the c-axis momentum transfer with maximum at integer $L = 0$, ±1, ±2 in an opposite fashion compared to the iron pnictides. Our results suggest a ferromagnetic interlayer coupling in $FeSe_{1-x}S_x$.

*Contact author: mw_ma@iphy.ac.cn

†Present address: Clarendon Laboratory, University of Oxford, Parks Road, Oxford OX1 3PU, United Kingdom.

‡Contact author: yuan.li@pku.edu.cn

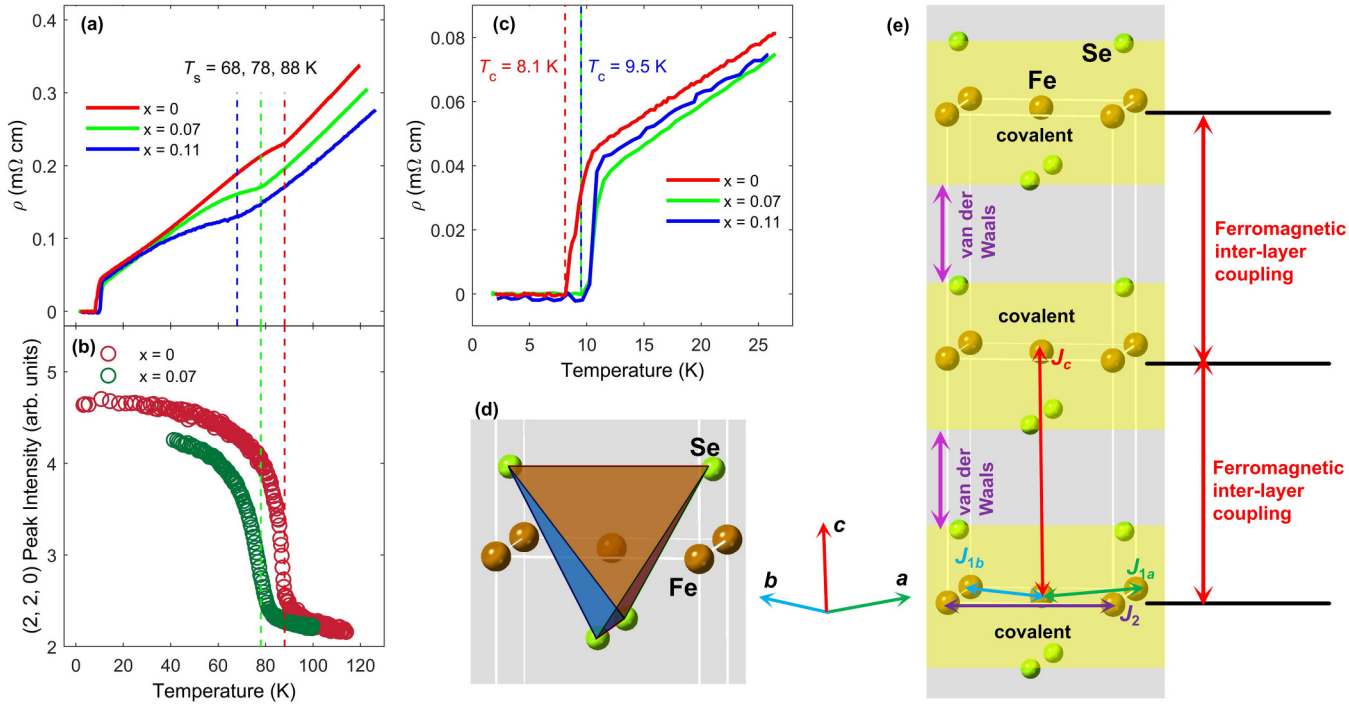

FIG. 1. (a) Temperature dependence of resistivity of $FeSe_{1-x}S_x$ for $x = 0$, 0.07, and 0.11 from $T = 2$ K to 120 K. (b) Temperature dependence of intensity of (2, 2, 0) Bragg peak of $FeSe_{1-x}S_x$ for $x = 0$ and 0.07. (c) Enlarged view of resistivity of $FeSe_{1-x}S_x$ for $x = 0$, 0.07, and 0.11 from $T = 2$ K to 25 K. (d) $FeSe_4$ tetrahedra. (e) Crystal structure of FeSe. The double arrows with different colors suggest interactions with each other, respectively.

II. EXPERIMENTAL METHODS

$FeSe_{1-x}S_x$ ($x = 0$, 0.07, and 0.11) single crystals have been grown by the chemical vapor transport technique [43] and co-aligned with a mosaic within 5° for all the sample arrays as shown in Fig. S1 (see Supplemental Material [44]). Figure 1(a) shows the temperature dependence of resistivity of $FeSe_{1-x}S_x$ ($x = 0$, 0.07, and 0.11). The nematic temperature T_s is gradually suppressed with increasing S doping. As displayed in the enlarged view of resistivity measurements [Fig. 1(c)], S doping causes a slight increase of T_c from 8.1 K ($x = 0$) to 9.5 K ($x = 0.07$ and 0.11).Here and throughout this article, the wave vector $\mathbf{Q}$ is expressed in reciprocal lattice units (r. l. u.) as (H, K, L). Using the orthorhombic notation of the 4-Fe Brillouin zone, the wave vector, expressed in inverse Angstrom, is $\mathbf{Q} = [(2\pi/a)H, (2\pi/b)K, (2\pi/c)L]$ with lattice parameters $a \approx b \approx 5.32$ Å and $c \approx 5.52$ Å.

The triple-axis INS experiments of FeSe mounted in the $(H, 0, L)$ scattering plane were carried out on a PUMA spectrometer at the Heinz Maier-Leibnitz Zentrum (MLZ), Technische Universität München, Garching, Germany. The triple-axis INS experiments of $FeSe_{0.93}S_{0.07}$ mounted in the $(H, 0, L)$ scattering plane were carried out on a 2T spectrometer at the Laboratoire Léon Brillouin, Saclay, France. The above measurements were done with $k_f = 2.662$ Å^{-1} using a focusing pyrolytic graphite (PG) monochromator and analyzer. Additional PG filters were placed between the sample and the analyzer to eliminate higher-order contaminations. The triple-axis INS experiments of $FeSe_{0.89}S_{0.11}$ mounted in the $(H, 0, L)$ scattering plane were carried out on an IN22 spectrometer with $k_f = 2.662$ Å^{-1} using the CryoPAD system with a Heusler $Cu_2MnAl(111)$ monochromator and analyzer at the Institut Laue-Langevin, Grenoble, France. The Cryopad capability is typically used to ensure that the sample is in a strictly zero magnetic field environment, thus avoiding errors due to flux inclusion and field expulsion in the superconducting phase of the sample [45]. Elastic neutron scattering for measuring the (2, 2, 0) Bragg peak of entire sample arrays was carried on a 4F1 spectrometer for FeSe at Laboratoire Léon Brillouin, Saclay, France and IN22 spectrometer for $FeSe_{0.93}S_{0.07}$ at Institut Laue-Langevin, Grenoble, France. They were both mounted in the $(H, K, 0)$ scattering plane. The intensity of (2, 2, 0) Bragg scattering of $FeSe_{1-x}S_x$ ($x = 0$ and 0.07) is enhanced across T_s due to the neutron extinction effect [46] as displayed in Fig. 1(b), indicating the homogeneity of each sample array.

The time-of-flight experiments of $FeSe_{0.93}S_{0.07}$ were performed on a 4SEASONS spectrometer [47] at the Material and Life Science Experimental Facility (MLF), Japan Proton Accelerator Research Complex (J-PARC), Japan. The 4SEASONS spectrometer has a multiple-E_i capability [48,49] with $E_i = 10$, 13.6, 19.4, 30.1, 52.1, and 116 meV, such that neutron scattering events with a series of different incident energies are recorded simultaneously. During the measurements at $T = 5$ K, 15 K, and 90 K, the sample was rotated about the vertical direction over a range of $\theta = \pm 55°$ and 0.5° steps, where the c axis is parallel to the incident neutron direction when $\theta = 0°$. Data accumulated at different angles were combined into a four-dimensional dataset, in which we used HORACE software packages for reduction and analysis. After

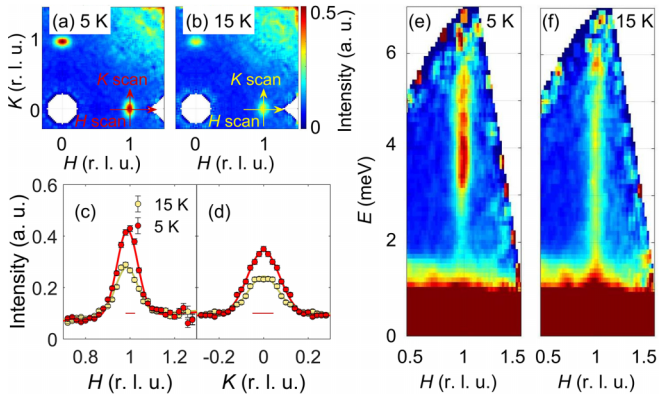

FIG. 2. (a) and (b) Constant-energy maps of $FeSe_{0.93}S_{0.07}$ obtained at $T = 5$ K and 15 K in the (H, K) momentum plane with $|L| \leqslant 0.2$ and $E = 4 \pm 1$ meV. (c) Longitudinal scan (H scan) at $T = 5$ K and 15 K with $E = 4 \pm 1$ meV, $|K| \leqslant 0.1$, and $|L| \leqslant 0.2$. (d) Transverse scan (K scan) at $T = 5$ K and 15 K with $E = 4 \pm 1$ meV, $|H - 1| \leqslant 0.1$, and $|L| \leqslant 0.2$. The horizontal red bars in (c) and (d) represent the expected momentum resolutions. Solid lines in (c) and (d) are Gaussian functions obtained by fitting the respective data. (e) and (f) Energy dependence of two-dimensional slices along the $\mathbf{Q} = (H, 0)$ direction at $T = 5$ K and 15 K with $|K| \leqslant 0.1$ and $|L| \leqslant 0.2$ for $FeSe_{0.93}S_{0.07}$. These data are obtained with incident energy $E_i = 13.6$ meV on a time-of-flight spectrometer 4SEASONS.

a careful alignment of the measured dataset with the crystallographic coordinate system using all available nuclear Bragg reflections, the entire dataset was downfolded into a minimal, physically independent sector of the three-dimensional momentum space using the point-group symmetry of the system.

III. RESULTS AND DISCUSSION

Figures 2(a) and 2(b) show constant-energy maps of spin excitations for $FeSe_{0.93}S_{0.07}$ in the superconducting state ($T = 5$ K) and nematic state ($T = 15$ K) at $E = 4$ meV in the (H, K) plane, where spin excitations are symmetrically located at $\mathbf{Q} = (\pm 1, 0)$ and $(0, \pm 1)$ with an elliptic distribution elongated in the transverse direction. The anisotropic distribution can also be displayed by transverse scan (K scan) and longitudinal scan (H scan) around $\mathbf{Q} = (1, 0)$ in Figs. 2(c) and 2(d) as indicated by the arrow in Figs. 2(a) and 2(b). Compared with the nematic state ($T = 15$ K), in the superconducting state an enhancement of the spin excitations around $E \approx 4$ meV is accompanied by a suppression of magnetic response below $E \approx 2.5$ meV as shown in Figs. 2(e) and 2(f), which is a hallmark of the spin resonance mode in agreement with previous INS studies on undoped FeSe [50–54]. The elongated distribution along the transverse direction of spin resonance in the (H, K) plane is consistent with the previous work on $Ba(Fe_{0.963}Ni_{0.037})_2As_2$ [55], $CaFe_{0.88}Co_{0.12}AsF$ [56], and $BaFe_2(As_{0.7}P_{0.3})_2$ [57], where the resonance is found to peak sharply at $\mathbf{Q}_{AF}$ along the longitudinal direction, but broadens along the transverse direction. Other similar constant-energy maps at $E = 2 - 6$ meV and energy-dependence measurements in the $E - K$ space at $T = 5$ K, 15 K, and 90 K are displayed in Fig. S2 (see Supplemental Material [44]). When

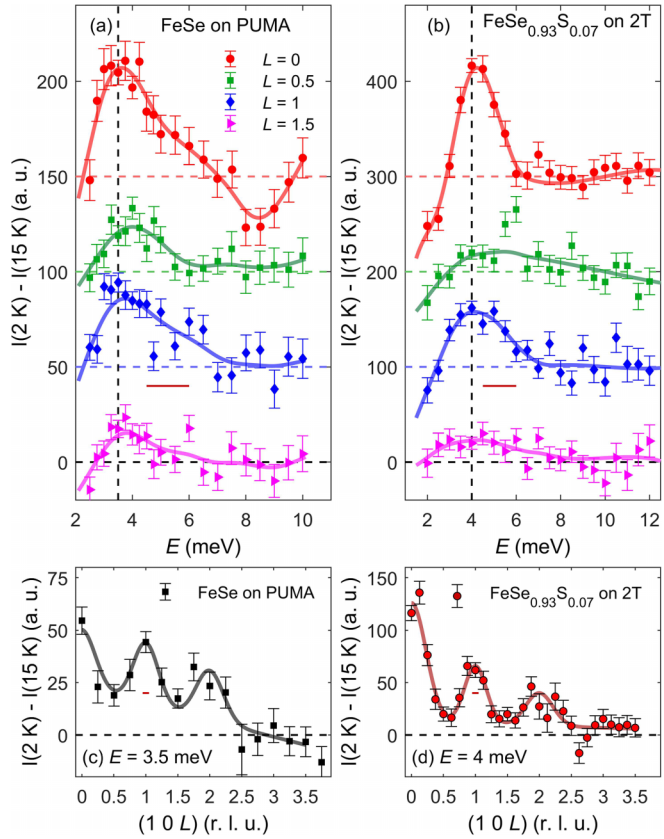

FIG. 3. (a) and (b) Temperature difference of spin excitations of FeSe and $FeSe_{0.93}S_{0.07}$ between superconducting state ($T = 2$ K) and nematic state ($T = 15$ K) at $\mathbf{Q} = (1, 0, L)$ with $L = 0$, 0.5, 1, and 1.5, respectively. (c) and (d) Temperature difference of spin excitations of FeSe and $FeSe_{0.93}S_{0.07}$ between the superconducting state ($T = 2$ K) and nematic state ($T = 15$ K) along the L direction at $E = 3.5$ and 4 meV, respectively. Solid lines are the guides to the eyes in (a) and (b) and multiple Gaussian functions fitted by the respective data in (c) and (d). These data in (a), (c) and in (b), (d) are obtained on triple-axis PUMA and 2T spectrometers, respectively. The horizontal red bars represent the expected momentum or energy resolutions, respectively.

entering the tetragonal state ($T = 90$ K), the magnetic signals at $\mathbf{Q} = (\pm 1, 0)$ and $(0, \pm 1)$ become weak and diffusive on a high background (BG), whereas the scattering signals at $\mathbf{Q} = (\pm 1, \pm 1)$ are heavily contaminated by the (1, 1, 0) phonon as displayed in Figs. S2(m)–S2(r).

After illustrating the anisotropic distribution of spin resonance in the (H, K) plane, we now turn to the L modulation of spin resonance. Figures 3(a) and 3(b) show the temperature difference of spin excitations of undoped FeSe and $FeSe_{0.93}S_{0.07}$ between the superconducting state ($T = 2$ K) and nematic state ($T = 15$ K) at $\mathbf{Q} = (1, 0, L)$ ($L = 0$, 0.5, 1, and 1.5). The spin resonance mode appears at $E_r \approx 3.5$ meV in FeSe, slightly enhanced at $E_r \approx 4$ meV in $FeSe_{0.93}S_{0.07}$. Notably, the spin resonance mode presents a stronger intensity at integer $L = 0$ and 1 than that at half-integer L. This L modulation of spin resonance can be further elucidated by the momentum scans along $\mathbf{Q} = (1, 0, L)$ at $E = 3.5$ meV for undoped FeSe [Fig. 3(c)] and $E = 4$ meV

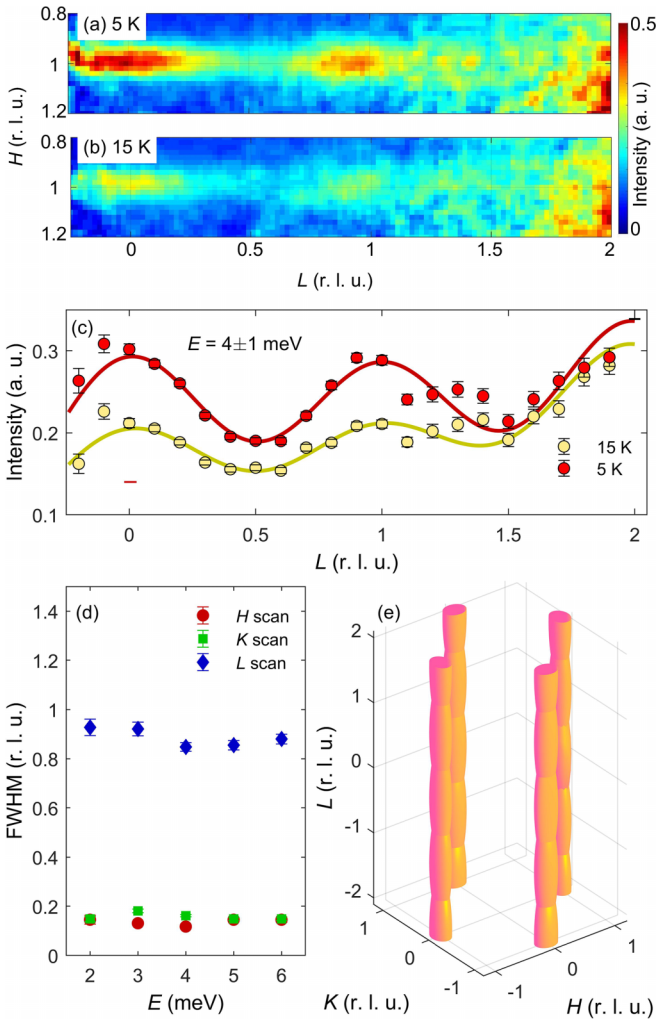

FIG. 4. (a) and (b) Constant-energy maps of $FeSe_{0.93}S_{0.07}$ obtained at $T = 5$ K and 15 K and in (H, L) momentum plane with $E = 4 \pm 1$ meV and $|K| \leqslant 0.1$. (c) L scans at $T = 5$ K and 15 K with $E = 4 \pm 1$ meV, $|K| \leqslant 0.1$, and $|H - 1| \leqslant 0.1$. The horizontal red bar represents the expected momentum resolution. Solid lines are Gaussian functions obtained by fitting the respective data. (d) Energy dependence of FWHM for H, K, and L scans fitted by gaussian functions (see Fig. S3 in Supplemental Material [44]). (e) The 3D distribution of spin excitation in momentum space using FWHM data from $E = 4 \pm 1$ meV.

for $FeSe_{0.93}S_{0.07}$ [Fig. 3(d)]. In addition, for a higher S-doped sample $FeSe_{0.89}S_{0.11}$, the similar L-modulated spin excitations at $E = 4$ meV in superconducting state are shown in Fig. S5(e) (See Supplemental Material [44]).

This strongly L-modulated spin resonance mode in superconducting state is closely related to the anisotropic distribution of low-energy spin excitations in momentum space in the nematic state ($T = 15$ K). Except for an intensity enhancement due to spin resonance, the anisotropic momentum distribution of spin excitations in the nematic state mimics that in the superconducting state as displayed in the constant energy maps in the (H, K) plane [Figs. 2(a) and 2(b)] and the (H, L) plane [Figs. 4(a) and 4(b)] as well as the L scans in Fig. 4(c). The spin excitations reveal elliptic distribution elongated in the transverse direction and a more elongated ellipse in the L direction in both the superconducting and nematic state. In order to quantitatively clarify the elliptic distribution of spin excitations in three-dimensional momentum space, momentum scans along the H, K, and L directions are presented in Figs. 2(c), 2(d), 4(c), and S3 (see Supplemental Material [44]), respectively. The intensity of spin excitations in the nematic state ($T = 15$ K) along the longitudinal (H), transverse (K), and L directions can be well fitted by Gaussian functions, revealing the FWHM values κ_H, κ_K, and κ_L as shown in Fig. 4(d). Comparing the FWHM along the H and K directions, κ_H and κ_K, respectively, one observes that the latter is slightly larger than the former. With a six-times-larger value κ_L than κ_K, the L dependence of intensity suggests a much more broadened distribution of spin excitations along the L direction, weakened with increasing energy and persisting up to $E \approx 15$ meV as shown in Figs. S3 and S4 (see Supplemental Material [44]). According to the FWHM we draw the schematic diagram of three-dimensional distribution of spin excitations in momentum space at $T = 15$ K and $E = 4$ meV as displayed in Fig. 4(e). The ellipsoids are periodically located at $\mathbf{Q} = (\pm 1, 0, L)$ or $(0, \pm 1, L)$ in a twinned sample where L is integer.

We now discuss the implications of our observed INS results. The feature of integer-L intensity enhancement of spin excitations in $FeSe_{1-x}S_x$ still survives in the nematic state, persisting up to $E \approx 15$ meV, and tells us that the spins in nearest-neighbor $FeSe_4$ layers are parallel and fluctuate in phase, which is opposite to the antiferromagnetic order in the parent compound of Fe pnictides with antiparallel spins of the nearest-neighbor layers along the c axis. A ferromagnetic-like interlayer coupling J_c has to be responsible for the integer-L intensity modulation in $FeSe_{1-x}S_x$. Even if FeSe does not order antiferromagnetically, it should not be far away from it. From a Heisenberg Hamiltonian similar to iron pnictides [58], the effective ferromagnetic interlayer coupling is estimated to be $J_c \sim 0.2$ meV with $J_c/J_{1a} \sim 0.3\%$ [59], which is much smaller than the antiferromagnetic interlayer coupling of FeTe $J_c \sim 1$ meV [60] (See Supplemental Material [44]).

The microscopic origin of the absence of the long-range stripe magnetic order in FeSe has been a topic of intense debate. One scenario is that the stripe magnetic order in FeSe is absent due to the development of other competing instabilities, considering mainly on the in-plane frustrated magnetic interactions [38–42]. From another point of view, a realistic three-dimensional antiferromagnetic order requires the spin correlations both in and out of plane. The spin-spin correlation length ξ is inversely proportional to the intrinsic momentum width of the signal peak κ_{real} with $\xi = 1/\kappa_{\text{real}}$ and $\kappa_{\text{real}} = \sqrt{\kappa^2_{\text{measured}} - \kappa^2_{\text{resolution}}}$, where κ_{measured} is the measured FWHM as shown in Fig. 4(d) and $\kappa_{\text{resolution}}$ is the momentum resolution as the red horizontal bar indicated in Figs. 2(c), 2(d), and 4(c) [61]. The spin-spin correlation lengths are therefore estimated to be $\xi_a \sim 7.7 \pm 0.4$ Å, $\xi_b \sim 6.5 \pm 0.2$ Å, and $\xi_c \sim 1.1 \pm 0.1$ Å. Considering the nearest Fe-Fe distance in the ab plane $d_{ab} \approx 2.66$ Å and the Fe-Fe distance along the c axis $d_c \approx 5.52$ Å, the spins of Fe atoms are more strongly correlated within the ab plane than that along the c axis indicated by $\xi_a/d_{ab} \sim 3$ and $\xi_c/d_c \sim 0.2$. The weak spin correlations along the c axis are in agreement with the small ferromagnetic interlayer coupling J_c. We believe that there might be a causal

relationship between the two anomalies (absence of magnetic order and ferromagnetic interlayer coupling) observed in the FeSe system.

IV. CONCLUSION

In conclusion, the anisotropic momentum distribution of spin resonance in $FeSe_{1-x}S_x$ mimics the low-energy spin excitations in its nematic phase where superconductivity arises, which implies the close relationship between superconductivity and magnetism. The strongly L-modulated spin resonance mode inherits the low-energy magnetic scattering in the nematic state with maximum intensity at integer L, indicating the ferromagnetic interlayer coupling in contrast to other iron-based superconductors. $FeSe_{1-x}S_x$ does not order antiferromagnetically, which is unusual among Fe-based materials. The ferromagnetic nature with weak interlayer coupling J_c and short spin-spin correlation length ξ_c might shed light on the absence of magnetic order in $FeSe_{1-x}S_x$.

ACKNOWLEDGMENTS

The work was supported by the National Key Research and Development of China (Grants No. 2022YFA1602800 and No. 2018YFA0704200), the National Natural Science Foundation of China (Grant No. 12004418), and the Strategic Priority Research Program of Chinese Academy of Sciences (Grant No. XDB25000000). One of the neutron scattering experiments was performed at the MLF, J-PARC, Japan, under a user program (No. 2018A0019).

[1] D. J. Scalapino, A common thread: The pairing interaction for unconventional superconductors, Rev. Mod. Phys. **84**, 1383 (2012).

[2] J. M. Tranquada, G. Xu, and I. A. Zaliznyak, Superconductivity, antiferromagnetism, and neutron scattering, J. Magn. Magn. Mater. **350**, 148 (2014).

[3] P. Dai, Antiferromagnetic order and spin dynamics in iron-based superconductors, Rev. Mod. Phys. **87**, 855 (2015).

[4] M. Eschrig, The effect of collective spin-1 excitations on electronic spectra in high-T_c superconductors, Adv. Phys. **55**, 47 (2006).

[5] S. Chi, A. Schneidewind, J. Zhao, L. W. Harriger, L. Li, Y. Luo, G. Cao, Z. Xu, M. Loewenhaupt, J. Hu, and P. Dai, Inelastic neutron-scattering measurements of a three-dimensional spin resonance in the FeAs-based $BaFe_{1.9}Ni_{0.1}As_2$ superconductor, Phys. Rev. Lett. **102**, 107006 (2009).

[6] S. Li, Y. Chen, S. Chang, J. W. Lynn, L. Li, Y. Luo, G. Cao, Z. Xu, and P. Dai, Spin gap and magnetic resonance in superconducting $BaFe_{1.9}Ni_{0.1}As_2$, Phys. Rev. B **79**, 174527 (2009).

[7] D. K. Pratt, A. Kreyssig, S. Nandi, N. Ni, A. Thaler, M. D. Lumsden, W. Tian, J. L. Zarestky, S. L. Bud'ko, P. C. Canfield, A. I. Goldman, and R. J. McQueeney, Dispersion of the superconducting spin resonance in underdoped and antiferromagnetic $BaFe_2As_2$, Phys. Rev. B **81**, 140510(R) (2010).

[8] C. Zhang, R. Yu, Y. Su, Y. Song, M. Wang, G. Tan, T. Egami, J. A. Fernandez-Baca, E. Faulhaber, Q. Si, and P. Dai, Measurement of a double neutron-spin resonance and an anisotropic energy gap for underdoped superconducting $NaFe_{0.985}Co_{0.015}As$ using inelastic neutron scattering, Phys. Rev. Lett. **111**, 207002 (2013).

[9] C. Stock, C. Broholm, J. Hudis, H. J. Kang, and C. Petrovic, Spin resonance in the d-wave superconductor $CeCoIn_5$, Phys. Rev. Lett. **100**, 087001 (2008).

[10] C. H. Lee, P. Steffens, N. Qureshi, M. Nakajima, K. Kihou, A. Iyo, H. Eisaki, and M. Braden, Universality of the dispersive spin-resonance mode in superconducting $BaFe_2As_2$, Phys. Rev. Lett. **111**, 167002 (2013).

[11] H. F. Fong, B. Keimer, D. Reznik, D. L. Milius, and I. A. Aksay, Polarized and unpolarized neutron-scattering study of the dynamical spin susceptibility of $YBa_2Cu_3O_7$, Phys. Rev. B **54**, 6708 (1996).

[12] J. M. Tranquada, P. M. Gehring, G. Shirane, S. Shamoto, and M. Sato, Neutron-scattering study of the dynamical spin susceptibility in $YBa_2Cu_3O_{6.6}$, Phys. Rev. B **46**, 5561 (1992).

[13] H. Chou, J. M. Tranquada, G. Shirane, T. E. Mason, W. J. L. Buyers, S. Shamoto, and M. Sato, Neutron-scattering study of spin fluctuations in superconducting $YBa_2Cu_3O_{6+x}$ ($x = 0.40$, 0.45, 0.50), Phys. Rev. B **43**, 5554 (1991).

[14] S. Pailhès, Y. Sidis, P. Bourges, C. Ulrich, V. Hinkov, L. P. Regnault, A. Ivanov, B. Liang, C. T. Lin, C. Bernhard, and B. Keimer, Two resonant magnetic modes in an overdoped high T_c superconductor, Phys. Rev. Lett. **91**, 237002 (2003).

[15] T. Xie, Y. Wei, D. Gong, T. Fennell, U. Stuhr, R. Kajimoto, K. Ikeuchi, S. Li, J. Hu, and H. Luo, Odd and even modes of neutron spin resonance in the bilayer iron-based superconductor $CaKFe_4As_4$, Phys. Rev. Lett. **120**, 267003 (2018).

[16] L. Capogna, B. Fauqué, Y. Sidis, C. Ulrich, P. Bourges, S. Pailhès, A. Ivanov, J. L. Tallon, B. Liang, C. T. Lin, A. I. Rykov, and B. Keimer, Odd and even magnetic resonant modes in highly overdoped $Bi_2Sr_2CaCu_2O_{8+\delta}$, Phys. Rev. B **75**, 060502(R) (2007).

[17] S. Pailhès, Y. Sidis, P. Bourges, V. Hinkov, A. Ivanov, C. Ulrich, L. P. Regnault, and B. Keimer, Resonant magnetic excitations at high energy in superconducting $YBa_2Cu_3O_{6.85}$, Phys. Rev. Lett. **93**, 167001 (2004).

[18] Y. Qiu, W. Bao, Y. Zhao, C. Broholm, V. Stanev, Z. Tesanovic, Y. C. Gasparovic, S. Chang, J. Hu, B. Qian, M. Fang, and Z. Mao, Spin gap and resonance at the nesting wave vector in superconducting $FeSe_{0.4}Te_{0.6}$, Phys. Rev. Lett. **103**, 067008 (2009).

[19] G. Friemel, J. T. Park, T. A. Maier, V. Tsurkan, Y. Li, J. Deisenhofer, H.-A. Krug von Nidda, A. Loidl, A. Ivanov, B. Keimer, and D. S. Inosov, Reciprocal-space structure and dispersion of the magnetic resonant mode in the superconducting phase of $Rb_xFe_{2-y}Se_2$ single crystals, Phys. Rev. B **85**, 140511(R) (2012).

[20] M. Ramazanoglu, J. Lamsal, G. S. Tucker, J.-Q. Yan, S. Calder, T. Guidi, T. Perring, R. W. McCallum, T. A. Lograsso, A. Kreyssig, A. I. Goldman, and R. J. McQueeney, Two-dimensional magnetic interactions in LaFeAsO, Phys. Rev. B **87**, 140509(R) (2013).

[21] N. Qureshi, P. Steffens, Y. Drees, A. C. Komarek, D. Lamago, Y. Sidis, L. Harnagea, H.-J. Grafe, S. Wurmehl, B. Büchner, and M. Braden, Inelastic neutron-scattering measurements of incommensurate magnetic excitations on superconducting LiFeAs single crystals, Phys. Rev. Lett. **108**, 117001 (2012).

[22] B. Pan, Y. Shen, D. Hu, Y. Feng, J. T. Park, A. D. Christianson, Q. Wang, Y. Hao, Z. Wo, H. Yin, T. A. Maier, and J. Zhao, Structure of spin excitations in heavily electron-doped $Li_{0.8}Fe_{0.2}$ODFeSe superconductors, Nat. Commun. **8**, 123 (2017).

[23] M. Ma, L. Wang, P. Bourges, Y. Sidis, S. Danilkin, and Y. Li, Low-energy spin excitations in $(Li_{0.8}Fe_{0.2})$ODFeSe superconductor studied with inelastic neutron scattering, Phys. Rev. B **95**, 100504(R) (2017).

[24] F.-C. Hsu, J.-Y. Luo, K.-W. Yeh, T.-K. Chen, T.-W. Huang, P. M. Wu, Y.-C. Lee, Y.-L. Huang, Y.-Y. Chu, D.-C. Yan, and M.-K. Wu, Superconductivity in the PbO-type structure FeSe, Proc. Natl. Acad. Sci. USA **105**, 14262 (2008).

[25] B. Lei, J. H. Cui, Z. J. Xiang, C. Shang, N. Z. Wang, G. J. Ye, X. G. Luo, T. Wu, Z. Sun, and X. H. Chen, Evolution of high-temperature superconductivity from a low-T_c phase tuned by carrier concentration in FeSe thin flakes, Phys. Rev. Lett. **116**, 077002 (2016).

[26] B. Lei, N. Z. Wang, C. Shang, F. B. Meng, L. K. Ma, X. G. Luo, T. Wu, Z. Sun, Y. Wang, Z. Jiang, B. H. Mao, Z. Liu, Y. J. Yu, Y. B. Zhang, and X. H. Chen, Tuning phase transitions in FeSe thin flakes by field-effect transistor with solid ion conductor as the gate dielectric, Phys. Rev. B **95**, 020503(R) (2017).

[27] T. P. Ying, M. X. Wang, X. X. Wu, Z. Y. Zhao, Z. Z. Zhang, B. Q. Song, Y. C. Li, B. Lei, Q. Li, Y. Yu, E. J. Cheng, Z. H. An, Y. Zhang, X. Y. Jia, W. Yang, X. H. Chen, and S. Y. Li, Discrete superconducting phases in FeSe-derived superconductors, Phys. Rev. Lett. **121**, 207003 (2018).

[28] X. F. Lu, N. Z. Wang, H. Wu, Y. P. Wu, D. Zhao, X. Z. Zeng, X. G. Luo, T. Wu, W. Bao, G. H. Zhang, F. Q. Huang, Q. Z. Huang, and X. H. Chen, Coexistence of superconductivity and antiferromagnetism in $(Li_{0.8}Fe_{0.2})$OHFeSe, Nat. Mater. **14**, 325 (2015).

[29] A. Krzton-Maziopa, E. V. Pomjakushina, V. Y. Pomjakushin, F. von Rohr, A. Schilling, and K. Conder, Synthesis of a new alkali metal-organic solvent intercalated iron selenide superconductor with $T_c \approx 45$ K, J. Phys.: Condens. Matter **24**, 382202 (2012).

[30] J. Guo, S. Jin, G. Wang, S. Wang, K. Zhu, T. Zhou, M. He, and X. Chen, Superconductivity in the iron selenide $K_xFe_2Se_2$($0 \leqslant x \leqslant 1.0$), Phys. Rev. B **82**, 180520(R) (2010).

[31] J. Guo, H. Lei, F. Hayashi, and H. Hosono, Superconductivity and phase instability of NH_3 free Na-intercalated $FeSe_{1-z}S_z$, Nat. Commun. **5**, 4756 (2014).

[32] T. P. Ying, X. L. Chen, G. Wang, S. F. Jin, T. T. Zhou, X. F. Lai, H. Zhang, and W. Y. Wang, Observation of superconductivity at 30−46 K in $A_xFe_2Se_2$(A = Li, Na, Ba, Sr, Ca, Yb, Eu), Sci. Rep. **2**, 426 (2012).

[33] Q. Wang, Z. Li, W. Zhang, Z. Zhang, J. Zhang, W. Li, H. Ding, Y. Ou, P. Deng, K. Chang, J. Wen, C. Song, K. He, J. Jia, S. Ji, Y. Wang, L. Wang, X. Chen, X. Ma, and Q. Xue, Interface-induced high-temperature superconductivity in single unit-cell FeSe films on $SrTiO_3$, Chin. Phys. Lett. **29**, 037402 (2012).

[34] S. He *et al.*, Phase diagram and electronic indication of high-temperature superconductivity at 65 K in single layer FeSe films, Nat. Mater. **12**, 605 (2013).

[35] J. Ge, Z. Lu, C. Liu, C. Gao, D. Qian, Q. Xue, Y. Liu, and J. Jia, Superconductivity above 100 K in single-layer FeSe films on doped $SrTiO_3$, Nat. Mater. **14**, 285 (2015).

[36] T. M. McQueen, A. J. Williams, P. W. Stephens, J. Tao, Y. Zhu, V. Ksenofontov, F. Casper, C. Felser, and R. J. Cava, Tetragonal-to-orthorhombic structural phase transition at 90 K in the superconductor $Fe_{1.01}Se$, Phys. Rev. Lett. **103**, 057002 (2009).

[37] S.-H. Baek, D. V. Efremov, J. M. Ok, J. S. Kim, J. van den Brink, and B. Büchner, Orbital-driven nematicity in FeSe, Nat. Mater. **14**, 210 (2015).

[38] R. Yu and Q. Si, Antiferroquadrupolar and Ising-nematic orders of a frustrated bilinear-biquadratic Heisenberg model and implications for the magnetism of FeSe, Phys. Rev. Lett. **115**, 116401 (2015).

[39] F. Wang, S. A. Kivelson, and D.-H. Lee, Nematicity and quantum paramagnetism in FeSe, Nat. Phys. **11**, 959 (2015).

[40] J. K. Glasbrenner, I. I. Mazin, H. O. Jeschke, P. J. Hirschfeld, R. M. Fernandes, and R. Valentí, Effect of magnetic frustration on nematicity and superconductivity in iron chalcogenides, Nat. Phys. **11**, 953 (2015).

[41] A. V. Chubukov, R. M. Fernandes, and J. Schmalian, Origin of nematic order in FeSe, Phys. Rev. B **91**, 201105(R) (2015).

[42] Y. Yamakawa, S. Onari, and H. Kontani, Nematicity and magnetism in FeSe and other families of Fe-based superconductors, Phys. Rev. X **6**, 021032 (2016).

[43] H. Li, M.-W. Ma, S.-B. Liu, F. Zhou, and X.-L. Dong, Structural and electrical transport properties of Cu-doped $Fe_{1x}Cu_xSe$ single crystals, Chin. Phys. B **29**, 127404 (2020).

[44] See Supplemental Material at http://link.aps.org/supplemental/10.1103/PhysRevB.110.174503 for raw data of inelastic neutron scattering.

[45] E. Lelièvre-Berna, E. Bourgeat-Lami, P. Fouilloux, B. Geffray, Y. Gibert, K. Kakurai, N. Kernavanois, B. Longuet, F. Mantegezza, M. Nakamura, S. Pujol, L.-P. Regnault, F. Tasset, M. Takeda, M. Thomas, and X. Tonon, Advances in spherical neutron polarimetry with cryopad, Phys. B: Condens. Matter **356**, 131 (2005).

[46] W. C. Hamilton, The effect of crystal shape and setting on secondary extinction, Acta Crystallogr. **10**, 629 (1957).

[47] R. Kajimoto *et al.*, The Fermi chopper spectrometer 4SEASONS at J-PARC, J. Phys. Soc. Jpn. **80**, SB025 (2011).

[48] M. Nakamura, R. Kajimoto, Y. Inamura, F. Mizuno, M. Fujita, T. Yokoo, and M. Arai, First demonstration of novel method for inelastic neutron scattering measurement utilizing multiple incident energies, J. Phys. Soc. Jpn. **78**, 093002 (2009).

[49] Y. Inamura, T. Nakatani, J. Suzuki, and T. Otomo, Development status of software Utsusemi for chopper spectrometers at MLF, J-PARC, J. Phys. Soc. Jpn. **82**, SA031 (2013).

[50] Y. Gu, Q. Wang, H. Wo, Z. He, H. C. Walker, J. T. Park, M. Enderle, A. D. Christianson, W. Wang, and J. Zhao, Frustrated magnetic interactions in FeSe, Phys. Rev. B **106**, L060504 (2022).

[51] Q. Wang, Y. Shen, B. Pan, Y. Hao, M. Ma, F. Zhou, P. Steffens, K. Schmalzl, T. R. Forrest, M. Abdel-Hafiez, X. Chen, D. A. Chareev, A. N. Vasiliev, P. Bourges, Y. Sidis, H. Cao, and J. Zhao, Strong interplay between stripe spin fluctuations,

nematicity and superconductivity in FeSe, Nat. Mater. **15**, 159 (2016).

[52] Q. Wang, Y. Shen, B. Pan, X. Zhang, K. Ikeuchi, K. Iida, A. D. Christianson, H. C. Walker, D. T. Adroja, M. Abdel-Hafiez, X. Chen, D. A. Chareev, A. N. Vasiliev, and J. Zhao, Magnetic ground state of FeSe, Nat. Commun. **7**, 12182 (2016).

[53] M. Ma, P. Bourges, Y. Sidis, Y. Xu, S. Li, B. Hu, J. Li, F. Wang, and Y. Li, Prominent role of spin-orbit coupling in FeSe revealed by inelastic neutron scattering, Phys. Rev. X **7**, 021025 (2017).

[54] T. Chen, Y. Chen, A. Kreisel, X. Lu, A. Schneidewind, Y. Qiu, J. T. Park, T. G. Perring, J. R. Stewart, H. Cao, R. Zhang, Y. Li, Y. Rong, Y. Wei, B. M. Andersen, P. J. Hirschfeld, C. Broholm, and P. Dai, Anisotropic spin fluctuations in detwinned FeSe, Nat. Mater. **18**, 709 (2019).

[55] M. G. Kim, G. S. Tucker, D. K. Pratt, S. Ran, A. Thaler, A. D. Christianson, K. Marty, S. Calder, A. Podlesnyak, S. L. Bud'ko, P. C. Canfield, A. Kreyssig, A. I. Goldman, and R. J. McQueeney, Magnon-like dispersion of spin resonance in Ni-doped $BaFe_2As_2$, Phys. Rev. Lett. **110**, 177002 (2013).

[56] M. Ma, P. Bourges, Y. Sidis, A. Ivanov, G. Chen, Z. Ren, and Y. Li, Low-energy spin excitations in the optimally doped $CaFe_{0.88}Co_{0.12}AsF$ superconductor studied with inelastic neutron scattering, Phys. Rev. B **107**, 184516 (2023).

[57] D. Hu, Z. Yin, W. Zhang, R. A. Ewings, K. Ikeuchi, M. Nakamura, B. Roessli, Y. Wei, L. Zhao, G. Chen, S. Li, H. Luo, K. Haule, G. Kotliar, and P. Dai, Spin excitations in optimally P-doped $BaFe_2(As_{0.7}P_{0.3})_2$ superconductor, Phys. Rev. B **94**, 094504 (2016).

[58] C. Wang, R. Zhang, F. Wang, H. Luo, L. P. Regnault, P. Dai, and Y. Li, Longitudinal spin excitations and magnetic anisotropy in antiferromagnetically ordered $BaFe_2As_2$, Phys. Rev. X **3**, 041036 (2013).

[59] R. Liu, M. B. Stone, S. Gao, M. Nakamura, K. Kamazawa, A. Krajewska, H. C. Walker, P. Cheng, R. Yu, Q. Si, P. Dai, and X. Lu, Nematic quantum disordered state in FeSe, arXiv:2401.05092.

[60] O. J. Lipscombe, G. F. Chen, C. Fang, T. G. Perring, D. L. Abernathy, A. D. Christianson, T. Egami, N. Wang, J. Hu, and P. Dai, Spin waves in the $(\pi, 0)$ magnetically ordered iron chalcogenide $Fe_{1.05}Te$, Phys. Rev. Lett. **106**, 057004 (2011).

[61] R. Kajimoto, K. Sato, Y. Inamura, and M. Fujita, Instrumental resolution of the chopper spectrometer 4SEASONS evaluated by Monte Carlo simulation, AIP Conf. Proc. **1969**, 050004 (2018).